American Mineralogist, Volume 97, pages 496–502, 2012

Falsterite, $Ca_2MgMn^{2+}_2(Fe^{2+}_{0.5}Fe^{3+}_{0.5})_4Zn_4(PO_4)_8(OH)_4(H_2O)_{14}$, a new secondary phosphate mineral from the Palermo No. 1 pegmatite, North Groton, New Hampshire

Anthony R. Kampf,[1,*] Stuart J. Mills,[2] William B. Simmons,[3] James W. Nizamoff,[3,4] and Robert W. Whitmore[5]

[1]Mineral Sciences Department, Natural History Museum of Los Angeles County, 900 Exposition Boulevard, Los Angeles, California 90007, U.S.A.
[2]Geosciences, Museum Victoria, GPO Box 666, Melbourne 3001, Australia
[3]Department of Earth and Environmental Science, University of New Orleans, 2000 Lakeshore Drive, New Orleans, Louisiana 70148, U.S.A.
[4]Omya, Inc., 39 Main Street, Proctor, Vermont 05765, U.S.A.
[5]934 S. Stark Highway, Weare, New Hampshire 03281, U.S.A.

Abstract

Falsterite, ideally $Ca_2MgMn^{2+}_2(Fe^{2+}_{0.5}Fe^{3+}_{0.5})_4Zn_4(PO_4)_8(OH)_4(H_2O)_{14}$, is a new mineral from the Palermo No. 1 pegmatite in North Groton, Grafton County, New Hampshire, U.S.A., and also occurs at the Estes pegmatite quarry, Baldwin, Cumberland County, Maine, U.S.A. It formed as the result of secondary alteration of primary triphylite and associated sphalerite. The crystals occur as very thin greenish-blue plates and rectangular laths, up to 0.7 mm in length, but no more than a few micrometers thick. Laths are flattened on {010}, elongate along [100], and exhibit lamellar twinning. The mineral is transparent and has a very pale greenish-blue streak, vitreous luster, Mohs hardness of about 2, flexible tenacity, irregular fracture, and perfect cleavage on {010}. The measured and calculated densities are 2.78(3) and 2.837 g/cm^3, respectively. It is optically biaxial (–), $\alpha = 1.575(10)$, $\beta = 1.600(5)$, $\gamma = 1.610(5)$ (white light), $2V_{meas} = 60(10)$, and $2V_{calc} = 63.8$. Falsterite exhibits strong dispersion, $r > v$. The optical orientation is $X = \mathbf{b}$, $Y \approx \mathbf{a}$, $Z \approx \mathbf{c}$. Pleochroism is pronounced: X, Z = colorless to very pale yellow, Y = blue green; $Y >> X \approx Z$. Electron-microprobe analyses (average of 7), with FeO and Fe_2O_3 apportioned and H_2O calculated on structural grounds, provided: CaO 6.36, MgO 2.13, MnO 8.10, ZnO 18.49, FeO 8.02, Fe_2O_3 8.90, Al_2O_3 0.02, P_2O_5 31.81, H_2O 16.17, total 100.00 wt%. The empirical formula (based on 50 O atoms) is $Ca_{2.02}Mg_{0.94}Mn^{2+}_{2.04}Fe^{2+}_{1.99}Fe^{3+}_{1.99}Zn_{4.05}P_{7.99}O_{32}(OH)_4(H_2O)_{14}$. The mineral dissolves very easily in cold, dilute HCl. Falsterite is monoclinic, $P2_1/c$, with the unit-cell parameters: $a = 6.3868(18)$, $b = 21.260(7)$, $c = 15.365(5)$ Å, $\beta = 90.564(6)$, $V = 2086.2(1.1)$ Å^3, and $Z = 2$. The eight strongest lines in the X-ray powder diffraction pattern are [d_{obs} in Å(I)(hkl)]: 12.86(34)(011); 10.675(100)(020); 4.834(12)(102,$\bar{1}$12); 4.043(18)($\bar{1}$32); 3.220(25)($\bar{1}$52); 3.107(14)(044); 2.846(19)($\bar{2}$22); 1.596(14)(0·12·4). The structure of falsterite ($R_1 = 6.42\%$ for 714 $F_o > 4\sigma F$) contains edge-sharing chains of $Fe^{2+}/Fe^{3+}O_6$ octahedra and corner-sharing chains of ZnO_4 tetrahedra along [100]. These chains are linked to one another by PO_4 tetrahedra, forming a sheet parallel to {010}. $Mn^{2+}O_6$ octahedra and CaO_7 polyhedra also link to this sheet, resulting in a thick slab. The slabs are bridged in the [010] direction by edge-sharing dimers of MgO_6 octahedra, which link to the slabs by sharing edges with ZnO_4 tetrahedra in adjacent slabs. The structures of falsterite and schoonerite, while topologically quite different, share similar components and structural features.

Keywords: Falsterite, new mineral, crystal structure, schoonerite, secondary phosphate, Palermo No. 1 pegmatite, New Hampshire, U.S.A.

Introduction

The new mineral described herein was discovered at the Palermo No. 1 pegmatite (Segeler et al. 1981; Whitmore and Lawrence 2004) in North Groton, Grafton County, New Hampshire, U.S.A. (43° 45.038′N 71° 53.378′W), by two of the authors (J.N. and R.W.W.) in 2003. The Palermo No. 1 pegmatite occurs in the Grafton pegmatite field on the west flank of the Kearsarge-Central Maine synclinorium (Billings 1956; Lyons et al. 1991). It is intruded into metasedimentary and metavolcanic rocks of the upper unit of the Lower Devonian Littleton formation, which were metamorphosed to sillimanite-muscovite grade during the Acadian orogeny (Francis et al. 1993).

The Palermo No. 1 pegmatite is a large, well-zoned beryl-phosphate subtype pegmatite (Černý and Ercit 2005), which has produced numerous large phosphate pods in the core margin and core zones, some of which reach nearly 12 m in maximum dimension. The Palermo No. 1 pegmatite is well known worldwide for its diverse suite of phosphate minerals, and most notably for its abundance of secondary phosphates. A total of over 140 mineral species have been identified from the pegmatite and, of these, over 90 are phosphates (Whitmore and Lawrence 2004). A pegmatite is also the source of aquamarine gem rough (McManus et al. 2008). Mineralogically, the Palermo No. 1 pegmatite resembles the equally famous

* E-mail: akampf@nhm.org

Hagendorf-Süd pegmatite in Bavaria, Germany (Strunz et al. 1975), which is also a beryl-phosphate subtype pegmatite.

The Palermo No. 1 pegmatite is the type locality for 10 new phosphate species, not including the new mineral described herein: whitlockite (Frondel 1941); wolfeite and xanthoxenite (Frondel 1949); palermoite (Frondel and Ito 1965); bjarebyite (Moore et al. 1973); whitmoreite (Moore et al. 1974); foggite, goedkenite, and samuelsonite (Moore et al. 1975); and schoonerite (Moore and Kampf 1977). It has been 35 yr since the last of these new species was described from the deposit.

The new species is named falsterite in honor of Alexander U. Falster (b. 1952) in recognition for his research on pegmatites and pegmatite minerals (e.g., columbite group minerals, tourmaline group minerals, REE minerals, and londonite). He has described the mineralogy and geochemistry of NYF-type pegmatites of the Wausau complex in Marathon County, Wisconsin, and the LCT-type pegmatites of Florence County, Wisconsin (cf. Falster 1981; Falster et al. 1996, 2000, 2001, 2011; Martin and Falster 1986). He has been a coauthor on the descriptions of seven new pegmatite minerals and is also a Scientific Research Technologist in the Department of Earth and Environmental Science, University of New Orleans (New Orleans, Louisiana, U.S.A.). The new mineral and name have been approved by the Commission on New Minerals, Nomenclature and Classification of the International Mineralogical Association (IMA 2011-061). No single specimen qualifies as the holotype; the description is based upon four cotype specimens, all of which are deposited in the Natural History Museum of Los Angeles County under catalog numbers 63565, 63566, 63567, and 63568.

Occurrence and paragenesis

Falsterite was found in a Zn- and Pb-rich phosphate–carbonate assemblage (Nizamoff et al. 2007) along the margin of a 1.5 m triphylite crystal in the core-margin of the Palermo No. 1 pegmatite. The triphylite crystal is rimmed on one side by a 10 to 30 cm thick rind of siderite, fluorapatite, and quartz. This carbonate-rich zone also contains minor amounts of sulfide minerals including pyrite, sphalerite, galena, and chalcopyrite. A significant portion of the sulfides have been altered by aqueous phosphate- and carbonate-bearing solutions, thereby resulting in the formation of numerous secondary Zn- and Pb-bearing phosphate and carbonate species. Minerals observed in direct association with falsterite include: messelite, mitridatite, phosphophyllite, quartz, schoonerite, siderite, smithsonite, and vivianite. Other secondary species observed in this assemblage include: cerussite, keckite, parascholzite, and pyromorphite.

Falsterite has also been confirmed by powder X-ray diffraction (PXRD) and energy-dispersive spectroscopy (EDS) to occur at the Estes quarry, Baldwin, Cumberland County, Maine, U.S.A. (Thompson et al. 2000) on a specimen collected by Gene Bearss. Associated minerals include: almandine, fairfieldite, muscovite, quartz, schoonerite, and sphalerite. This material was not used in the characterization of the species.

Physical and optical properties

Falsterite crystals occur as very thin greenish-blue plates and rectangular laths up to 0.7 mm in length, but no more than a few micrometers thick (Figs. 1 and 2). Laths are flattened on {010} and elongate along [100]; they exhibit the forms {010}, {100}, and {001}. Lamellar twinning is common.

Falsterite is greenish blue and has a very pale greenish-blue streak. Crystals are transparent and have vitreous luster. Falsterite does not fluoresce in long- or short-wave ultraviolet light. The Mohs hardness is about 2, the tenacity is flexible, the fracture is irregular, and crystals exhibit one perfect cleavage on {010}. The density measured by sink-float in an aqueous solution of lithium metatungstate is 2.78(3) g/cm^3. The calculated density based on the empirical formula and single-crystal unit cell is 2.837 g/cm^3. Falsterite dissolves very easily in cold, dilute HCl.

Optically, falsterite is biaxial negative, with $\alpha = 1.575(10)$,

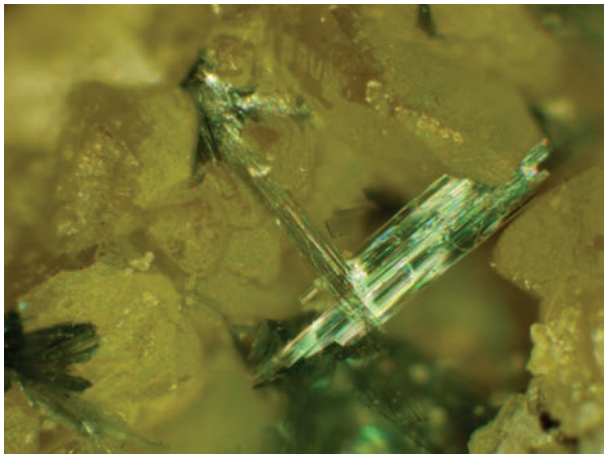

Figure 1. Falsterite blades on siderite from the Palermo No. 1 pegmatite (FOV = 1 mm).

Figure 2. SEM image of falsterite from the Palermo No. 1 pegmatite.

$\beta = 1.600(5)$, $\gamma = 1.610(5)$, measured in white light. The $2V$, measured directly by conoscopic observation, is 60(10)°. The calculated $2V$ is 63.8°. Falsterite exhibits strong dispersion, $r > v$. The optical orientation is $X = \mathbf{b}$, $Y \approx \mathbf{a}$, $Z \approx \mathbf{c}$ and pleochroism is pronounced: X, Z = colorless to very pale yellow, Y = blue green; $Y >> X \approx Z$. Note that crystals exhibit lamellar twinning and mosaic texture, resulting in somewhat undulatory extinction. The extreme thinness of the plates made it difficult to measure α. The thinness of the plates, coupled with the strong dispersion, resulted in very diffuse isogyres in conoscopic view. Consequently, the uncertainties in the measurements of α and $2V$ are quite large. The strong dispersion also results in anomalous strong red to orange colors when flat-lying blades are viewed in white light under crossed polars.

Chemical composition

Seven chemical analyses were carried out using an ARL-SEMQ electron microprobe in the Department of Earth and Environmental Science, University of New Orleans (WDS mode, 15 kV, 10 mA, and 1.5 μm beam diameter). FeO and Fe_2O_3 have been apportioned in accord with the structure determination. Insufficient material is available for direct water determination. The H_2O content is calculated by stoichiometry based upon the structure determination. Analytical data and standards are given in Table 1.

The empirical formula (based on 50 O atoms) is $Ca_{2.02}Mg_{0.94}Mn^{2+}_{2.04}Fe^{2+}_{1.99}Fe^{3+}_{1.99}Zn_{4.05}P_{7.99}O_{32}(OH)_4(H_2O)_{14}$. The simplified formula is $Ca_2MgMn^{2+}_2Fe^{2+}_2Fe^{3+}_2Zn_4(PO_4)_8(OH)_4(H_2O)_{14}$, which requires CaO 6.30, MgO 2.27, MnO 7.97, FeO 8.08, Fe_2O_3 8.98, ZnO 18.30, P_2O_5 31.91, H_2O 16.20, total 100.00 wt%.

The Gladstone-Dale compatibility index $1 - (K_P/K_C)$ as defined by Mandarino (1981) provides a measure of the consistency among the average index of refraction, calculated density, and chemical composition. For falsterite, the compatibility index is 0.043 based on the empirical formula, within the range of good compatibility.

X-ray crystallography and structure refinement

Both powder and single-crystal X-ray studies were carried out using a Rigaku R-Axis Rapid II curved imaging plate microdiffractometer, with monochromatized Mo$K\alpha$ radiation. For the powder-diffraction study, a Gandolfi-like motion on the φ and ω axes was used to randomize the sample and observed *d*-spacings and intensities were derived by profile fitting using JADE 9.3 software. The powder data are presented in Table 2. The intensities of most of the calculated powder lines based on the structure determination are somewhat low relative to the observed peaks; however, whole pattern fitting using JADE 9.3 demonstrated generally good agreement between the observed and calculated patterns, except for the intensities of the two lowest angle lines, corresponding to the (011) and (020) reflections, which modeled significantly too low and too high, respectively. We suspect that these anomalies may be related to the extreme thinness of the crystals on {010}. Although preferred orientation is not expected to be a factor, applying an empirical correction for preferred orientation significantly improved the fit of the (011) and (020) lines. Unit-cell parameters refined from the powder data using whole pattern fitting are: $a = 6.373(5)$, $b = 21.257(5)$, $c = 15.336(5)$ Å, $\beta = 90.58(3)°$, and $V = 2077.3(1.8)$ Å^3.

The Rigaku CrystalClear software package was used for processing the single-crystal X-ray diffraction data, including the application of an empirical absorption correction. The extreme thinness and high mosaicity of the crystal limited the data to a maximum θ of 17.20°, yielded a high R_{int} of 0.22, and probably is the cause of the relatively high-displacement parameters for

Table 1. Analytical results for falsterite

Constant	wt%	Range	S.D.	Standard
CaO	6.36	6.21–6.52	0.12	Fluorapatite
MgO	2.13	2.01–2.32	0.13	Triphylite
FeO	(16.04)	15.83–16.42	0.21	Triphylite
FeO*	8.02			
Fe_2O_3*	8.90			
MnO	8.10	7.77–8.32	0.19	Lithiophilite
ZnO	18.49	18.30–18.49	0.19	ZnO
Al_2O_3	0.02	0.01–0.04	0.01	Amblygonite
P_2O_5	31.81	31.65–31.96	0.13	Triphylite
H_2O†	16.17			
Total	100.00			

* Apportioned in accord with the structure.
† Calculated from the structure.

Table 2. Powder X-ray data for falsterite

I_{obs}	d_{obs}	d_{calc}	I_{calc}	*h k l*	I_{obs}	d_{obs}	d_{calc}	I_{calc}	*h k l*
34	12.86(3)	12.4528	4	0 1 1			2.6603	1	0 4 5
100	10.675(8)	10.6300	100	0 2 0			2.6149	1	2 2 3
2	7.756(31)	7.6821	1	0 0 2	8	2.586(29)	2.6123	1	0 7 3
1	6.467(34)	6.4351	1	0 3 1			2.5853	2	$\bar{2}$ 4 2
		5.1707	1	$\bar{1}$ 2 1			2.5716	1	2 4 2
		4.9790	1	0 1 3			2.5534	1	2 5 0
		4.8874	1	$\bar{1}$ 0 2			2.5408	1	$\bar{2}$ 3 3
12	4.834(17)	4.8072	1	$\bar{1}$ 1 2			2.5213	1	2 3 3
		4.7632	1	1 1 2	9	2.504(21)	2.5115	1	0 8 2
		4.6139	1	0 2 3			2.4906	2	0 5 5
7	4.361(11)	4.3709	2	0 4 2			2.4675	1	$\bar{2}$ 0 4
8	4.162(6)	4.1509	1	0 3 3			2.4277	1	2 1 4
18	4.043(5)	4.0498	5	$\bar{1}$ 3 2	9	2.422(1)	2.4243	1	$\bar{1}$ 8 1
		4.0234	3	1 3 2			2.4173	2	2 5 2
3	3.737(15)	3.7799	1	0 1 4			2.4056	1	2 4 3
		3.6879	1	0 4 3			2.4036	1	$\bar{2}$ 2 4
6	3.611(5)	3.6125	4	0 2 4			2.3069	1	0 4 6
		3.5976	1	1 4 2			2.2923	1	$\bar{2}$ 5 3
		3.3769	1	0 3 4	7	2.276(1)	2.2712	2	$\bar{2}$ 6 2
		3.2774	2	1 0 4			2.2619	1	2 6 2
		3.2715	2	0 5 3	4	2.182(4)	2.1601	1	0 7 5
		3.2667	2	$\bar{1}$ 1 4			2.1307	1	$\bar{1}$ 9 2
		3.2391	1	1 1 4	5	2.113(2)	2.1118	2	2 7 2
		3.2212	3	$\bar{1}$ 5 2	4	2.078(2)	2.0800	1	$\bar{1}$ 5 6
25	3.220(3)	3.2176	6	0 6 2			2.0755	1	0 6 6
		3.2079	3	1 5 2	7	1.976(1)	1.9772	2	$\bar{2}$ 8 2
		3.2035	1	$\bar{1}$ 4 3			1.9710	1	2 8 2
		3.1132	5	0 4 4			1.9577	1	0 7 6
14	3.107(8)	3.0872	1	2 1 1	4	1.916(1)	1.9205	1	0 0 8
		3.0582	1	2 2 0			1.9127	2	0 1 8
		3.0412	1	0 1 5	7	1.855(2)	1.8626	1	$\bar{3}$ 1 4
		2.9940	1	2 2 1	5	1.729(3)	1.7466	1	$\bar{2}$ 6 6
		2.9590	1	$\bar{2}$ 0 2	2	1.663(2)	1.6635	1	2 7 6
		2.9520	1	0 2 5	7	1.634(1)	1.6338	1	2 1 8
		2.9139	1	0 6 3			1.6088	1	0 12 4
		2.8651	3	$\bar{2}$ 3 1	14	1.596(1)	1.6018	2	$\bar{2}$ 8 6
		2.8558	3	2 3 1			1.5966	1	2 3 8
19	2.846(3)	2.8506	1	$\bar{2}$ 2 2			1.5921	2	4 1 0
		2.8503	1	0 5 4			1.5784	1	$\bar{2}$ 4 8
		2.8192	3	0 3 5	4	1.521(1)	1.5211	1	2 9 6
11	2.691(2)	2.7372	2	2 4 0					
		2.6997	2	$\bar{2}$ 1 3					
		2.6987	2	$\bar{2}$ 4 1					
		2.6909	1	2 4 1					

all atoms. The structure was solved by direct methods using SIR2004 (Burla et al. 2005). SHELXL-97 software (Sheldrick 2008) was used, with neutral atom scattering factors, for the refinement of the structure. Direct methods provided the locations of all cation sites except that of Mg and all but two of the O sites (OW25 and OW26). The Mg, OW25, and OW26 sites were located on difference-Fourier maps. The OW25 and OW26 sites were assigned half occupancy. The Mg site was also initially assigned half occupancy; however, because this resulted in a much lower U_{eq} (0.025) than for the other sites in the structure, the occupancy of the Mg site was subsequently refined with joint occupancy by Mg and Zn, totaling half occupancy. The occupancy refined to 0.464 Mg and 0.036 Zn, which corresponds to ($Mg_{0.93}Zn_{0.07}$) apfu. This is in reasonable agreement with the empirical formula, in which there is an excess of 0.05 Zn and a deficiency of 0.05 Mg.

The details of the data collection and the final structure refinement are provided in Table 3. The final fractional coordinates and atom displacement parameters are provided in Table 4. Selected interatomic distances are listed in Table 5 and bond valences in Table 6. (A CIF and a table of observed and calculated structure factors are available[1].)

[1] Deposit item AM-12-027, CIF and structure factors deposit table. Deposit items are available two ways: For a paper copy contact the Business Office of the Mineralogical Society of America (see inside front cover of recent issue) for price information. For an electronic copy visit the MSA web site at http://www.minsocam.org, go to the *American Mineralogist* Contents, find the table of contents for the specific volume/issue wanted, and then click on the deposit link there.

TABLE 3. Data collection and structure refinement details for falsterite

Diffractometer	Rigaku R-Axis Rapid II
X-ray radiation/power	Mo$K\alpha$ (λ = 0.71075 Å)
Temperature	298(2) K
Structural formula	$Ca_2(Mg_{0.93}Zn_{0.07})Mn_2^{2+}(Fe_{0.5}^{2+}Fe_{0.5}^{3+})_4Zn_4(PO_4)_8(OH)_4(H_2O)_{14}$
Space group	$P2_1/c$
Unit-cell dimensions	a = 6.3868(18) Å
	b = 21.260(7) Å
	c = 15.365(5) Å
	β = 90.564(6)°
V	2086.2(11) Å^3
Z	2
Density (for above formula)	2.832 g/cm^3
Absorption coefficient	4.900 mm^{-1}
F(000)	1760
Crystal size	250 × 60 × 1 µm
θ range	3.1 to 17.20°
Index ranges	$-5 \le h \le 5$, $-17 \le k \le 17$, $-12 \le l \le 12$
Reflections collected/unique	10009/1211 [R_{int} = 0.22]
Reflections with $F_o > 4\sigma F$	714
Completeness to θ = 17.20°	95.6%
Max. and min. transmission	0.995 and 0.374
Refinement method	Full-matrix least-squares on F^2
Parameters refined	336
GoF	1.012
Final R indices [$F_o > 4\sigma(F)$]	R_1 = 0.0642, wR_2 = 0.1411
R indices (all data)	R_1 = 0.1190, wR_2 = 0.1680
Extinction coefficient	0.0008(6)
Largest diff. peak/hole	+0.87/–0.61 e A^{-3}

Notes: $R_{int} = \Sigma|F_o^2 - F_o^2(\text{mean})|/\Sigma[F_o^2]$. GoF = $S = \{\Sigma[w(F_o^2 - F_c^2)^2]/(n-p)\}^{1/2}$. $R_1 = \Sigma||F_o| - |F_c||/\Sigma|F_o|$. $wR_2 = \{\Sigma[w(F_o^2 - F_c^2)^2]/\Sigma[w(F_o^2)^2]\}^{1/2}$. $w = 1/[\sigma^2(F_o^2) + (aP)^2 + bP]$ where a is 0.0915, b is 0, and P is $[2F_c^2 + \text{Max}(F_o^2,0)]/3$.

TABLE 4. Fractional coordinates and atom displacement parameters (Å^2) for falsterite

	x/a	y/b	z/c	U_{eq}	U_{11}	U_{22}	U_{33}	U_{23}	U_{13}	U_{12}
Ca	0.5368(10)	0.3734(3)	0.6401(4)	0.051(2)	0.051(5)	0.056(5)	0.046(5)	0.000(4)	0.001(4)	–0.004(4)
P1	0.0410(16)	0.2979(5)	0.5927(7)	0.052(3)	0.036(8)	0.063(8)	0.059(8)	–0.004(7)	0.001(7)	0.001(5)
P2	0.5452(15)	0.2914(5)	0.4394(6)	0.047(3)	0.045(9)	0.049(8)	0.048(7)	0.003(6)	0.020(7)	0.002(5)
P3	0.0352(17)	0.1305(4)	0.3659(7)	0.049(3)	0.055(8)	0.052(8)	0.041(8)	0.003(6)	0.017(7)	–0.005(5)
P4	0.5490(18)	0.1327(4)	0.6749(7)	0.052(3)	0.063(9)	0.050(8)	0.044(8)	0.008(6)	–0.014(7)	0.000(6)
Mg*	0.293(3)	0.0428(8)	0.5181(12)	0.041(10)	0.023(14)	0.054(15)	0.047(16)	0.014(10)	0.018(9)	0.010(9)
Zn1	0.2931(6)	0.18160(17)	0.5218(3)	0.0561(15)	0.045(3)	0.082(3)	0.042(3)	–0.002(2)	0.002(2)	0.005(2)
Zn2	0.7949(6)	0.18224(15)	0.5227(2)	0.0498(14)	0.048(3)	0.053(3)	0.048(3)	–0.003(2)	0.001(2)	0.003(2)
Fe1	0.2933(7)	0.24592(19)	0.2653(3)	0.0454(16)	0.043(3)	0.051(3)	0.042(4)	–0.004(2)	0.004(3)	0.004(2)
Fe2	0.7899(7)	0.2456(2)	0.2650(3)	0.0473(16)	0.047(4)	0.050(3)	0.045(4)	0.001(2)	0.002(3)	0.000(2)
Mn	0.0451(8)	0.3486(2)	0.3910(3)	0.0533(19)	0.045(4)	0.066(4)	0.049(4)	–0.004(3)	0.008(3)	0.000(3)
Ca	0.5369(10)	0.3734(3)	0.6401(4)	0.051(2)	0.051(5)	0.056(5)	0.045(5)	–0.001(4)	0.002(4)	–0.004(4)
O1	0.035(3)	0.3514(8)	0.5282(12)	0.048(6)	0.055(16)	0.029(13)	0.058(16)	0.030(12)	0.011(12)	0.012(11)
O2	0.238(3)	0.1993(8)	0.1496(12)	0.046(6)	0.027(15)	0.058(15)	0.052(14)	0.022(12)	0.000(12)	–0.012(10)
O3	0.839(3)	0.2045(8)	0.1485(12)	0.045(6)	0.033(15)	0.053(14)	0.048(15)	0.002(11)	0.005(13)	–0.017(11)
O4	0.043(3)	0.2323(8)	0.5431(11)	0.037(5)	0.034(14)	0.047(14)	0.030(14)	–0.006(11)	0.013(11)	–0.009(10)
O5	0.555(3)	0.3510(10)	0.4912(13)	0.049(6)	0.018(13)	0.073(17)	0.057(16)	0.003(13)	–0.004(11)	–0.002(11)
O6	0.742(3)	0.2857(8)	0.3839(11)	0.039(6)	0.020(15)	0.075(16)	0.023(14)	0.016(10)	–0.004(12)	0.000(10)
O7	0.543(3)	0.2318(9)	0.4964(13)	0.050(6)	0.030(15)	0.050(15)	0.069(17)	–0.011(13)	–0.017(12)	0.006(11)
O8	0.338(3)	0.2870(8)	0.3810(13)	0.052(6)	0.015(14)	0.058(15)	0.081(18)	–0.006(12)	–0.005(13)	0.005(11)
O9	0.837(4)	0.1323(8)	0.4209(12)	0.056(7)	0.08(2)	0.058(16)	0.028(15)	0.008(11)	–0.008(15)	–0.018(12)
O10	0.032(3)	0.0753(9)	0.3023(14)	0.071(7)	0.10(2)	0.047(16)	0.061(16)	–0.008(13)	–0.034(14)	–0.005(13)
O11	0.045(3)	0.1944(9)	0.3197(12)	0.052(6)	0.042(15)	0.050(16)	0.063(16)	0.032(12)	0.012(12)	0.000(11)
O12	0.232(3)	0.1246(9)	0.4285(13)	0.066(7)	0.073(19)	0.071(17)	0.054(17)	–0.009(12)	–0.015(16)	0.008(12)
O13	0.373(3)	0.1265(9)	0.6114(15)	0.073(8)	0.041(17)	0.075(18)	0.10(2)	–0.003(14)	–0.030(18)	–0.004(11)
O14	0.544(3)	0.0826(9)	0.7455(13)	0.052(6)	0.043(15)	0.054(15)	0.060(16)	–0.013(14)	0.013(12)	0.018(11)
O15	0.541(3)	0.2005(10)	0.7142(12)	0.067(7)	0.09(2)	0.063(17)	0.045(16)	–0.003(13)	0.022(14)	0.015(13)
O16	0.762(4)	0.1294(9)	0.6212(13)	0.064(7)	0.09(2)	0.064(18)	0.043(17)	0.017(11)	0.017(15)	0.029(12)
OH17	0.539(3)	0.1846(7)	0.2777(11)	0.043(6)	0.045(15)	0.027(13)	0.056(15)	–0.001(10)	–0.013(11)	0.003(10)
OH18	0.038(3)	0.3076(8)	0.2585(11)	0.050(6)	0.073(17)	0.047(14)	0.029(14)	–0.005(10)	0.000(12)	0.015(11)
OW19	0.247(3)	0.4291(8)	0.3607(12)	0.061(7)	0.103(19)	0.033(13)	0.048(15)	0.015(10)	0.028(13)	–0.005(11)
OW20	0.786(3)	0.4237(9)	0.3902(12)	0.058(6)	0.040(15)	0.077(17)	0.055(16)	–0.011(11)	–0.007(12)	–0.008(11)
OW21	0.425(3)	0.4516(9)	0.7457(14)	0.078(7)	0.091(19)	0.051(15)	0.093(19)	0.006(13)	0.027(15)	–0.006(13)
OW22	0.347(3)	0.4546(8)	0.5593(14)	0.073(7)	0.085(19)	0.052(15)	0.083(18)	0.012(13)	–0.007(14)	0.009(12)
OW23	0.854(3)	0.4405(9)	0.6465(13)	0.063(7)	0.054(16)	0.060(15)	0.077(17)	0.000(12)	0.029(13)	–0.006(11)
OW24	0.426(4)	0.9660(9)	0.5684(16)	0.090(8)	0.070(19)	0.063(17)	0.14(2)	–0.016(15)	0.031(17)	0.004(13)
OW25*	0.048(7)	0.0363(16)	0.596(3)	0.052(13)	0.03(3)	0.04(3)	0.08(4)	0.01(2)	–0.03(3)	0.00(2)
OW26*	0.146(8)	0.9872(18)	0.423(2)	0.054(13)	0.09(4)	0.06(3)	0.01(3)	–0.02(2)	0.01(3)	0.03(3)

* The refined Mg site occupancy is Mg 0.464 and Zn 0.036(19); OW25 and OW26 sites are assigned 0.5 occupancy.

Description of the structure

The structure of falsterite (Fig. 3) contains edge-sharing chains of $Fe^{2+}/Fe^{3+}O_6$ octahedra and corner-sharing chains of ZnO_4 tetrahedra along **a**. These chains are linked to one another by PO_4 tetrahedra, forming a sheet parallel to {010}. $Mn^{2+}O_6$ octahedra and CaO_7 polyhedra also link to this sheet, resulting in a thick slab. The slabs are bridged in the [010] direction by edge-sharing dimers of MgO_6 octahedra, which link to the slabs by sharing edges with ZnO_4 tetrahedra in adjacent slabs. The Mg site refines to only half occupancy, as do the OW25 and OW26 sites of the MgO_6 octahedra in adjacent dimers (which are only 1.35 Å apart). This suggests that alternate dimers in the [100] direction are vacant, except for the OW24 sites corresponding to their shared edge. An extensive network of hydrogen bonds further links the slabs.

The mixed-valent (Fe^{2+}/Fe^{3+}) nature of the Fe1 and Fe2 sites is clearly indicated by bond-valence balance arguments and is reflected in the average Fe–O bond lengths for the sites, which are intermediate between normal Fe^{2+}–O and Fe^{3+}–O bond lengths. The Fe–O bond strengths used for the bond valence analysis in Table 7 are based on occupancy of the Fe1 and Fe2 sites by ½Fe^{2+} and ½Fe^{3+}.

The structures of falsterite and schoonerite (Kampf 1977) are topologically quite different, but they share similar components and structural features (Fig. 3). Both structures contain thick slabs composed of linkages of Fe^{2+}, Fe^{3+}, and Mn^{2+} octahedra, Zn polyhedra (ZnO_4 tetrahedra in falsterite and ZnO_5 trigonal bipyramids in schoonerite), and PO_4 tetrahedra. The most prominent feature in each slab is an edge-sharing chain of FeO_6 octahedra, but the chains differ in that, in schoonerite, the chain contains only Fe^{2+}, while that in falsterite contains both Fe^{2+} and Fe^{3+}. In schoonerite, additional $Fe^{3+}O_6$ octahedra link the chains to one another by corner sharing.

An interesting consequence is that falsterite and schoonerite exhibit strikingly different colors. The strong greenish-blue pleochroic color of falsterite parallel to [100] is clearly related

Table 5. Selected bond distances (Å) in falsterite

P1-O1	1.508(18)	Fe1-O8	1.999(20)	Mg-OW24	1.99(3)
P1-O2	1.524(18)	Fe1-OH17	2.048(17)	Mg-OW25	1.99(5)
P1-O3	1.559(19)	Fe1-O2	2.063(20)	Mg-OW26	2.09(5)
P1-O4	1.590(18)	Fe1-OH18	2.096(18)	Mg-O12	2.25(3)
<P-O>	1.545	Fe1-O11	2.105(19)	Mg-OW24	2.25(3)
		Fe1-O15	2.108(20)	Mg-O13	2.34(3)
P2-O5	1.496(20)	<Fe-O>	2.084	<Mg-O>	2.19
P2-O6	1.529(19)				
P2-O7	1.541(20)	Fe2-O3	2.019(19)	Hydrogen bonds (D-A)	
P2-O8	1.594(19)	Fe2-O6	2.042(19)	OH17-OW21	3.02(3)
<P-O>	1.540	Fe2-OH18	2.062(20)	OH18-O16	3.04(2)
		Fe2-OH17	2.072(18)	OW19-O14	2.62(3)
P3-O9	1.527(21)	Fe2-O15	2.102(22)	OW19-OW23	2.85(3)
P3-O10	1.527(23)	Fe2-O11	2.128(19)	OW20-O14	2.70(3)
P3-O11	1.535(19)	<Fe-O>	2.081	OW20-OW22	2.83(3)
P3-O12	1.581(22)			OW21-O10	2.73(3)
<P-O>	1.543	Mn-O1	2.111(2)	OW21-O14	2.80(3)
		Mn-OW19	2.195(18)	OW22-O1	3.00(3)
P4-O13	1.489(22)	Mn-OH18	2.215(18)	OW22-OW20	2.83(3)
P4-O14	1.521(20)	Mn-O8	2.291(18)	OW23-O10	2.66(3)
P4-O15	1.564(21)	Mn-OW20	2.302(19)	OW23-OW19	2.85(3)
P4-O16	1.599(22)	Mn-O6	2.356(17)	OW24-O9	2.69(3)
<P-O>	1.543	<Mn-O>	2.272	OW24-OW21	3.02(3)
				OW25-O10	2.89(5)
Zn1-O13	1.874(22)	Ca-O5	2.341(21)	OW25-O16	2.72(5)
Zn1-O12	1.914(20)	Ca-OW21	2.436(21)	OW26-O10	2.73(4)
Zn1-O4	1.958(18)	Ca-OW22	2.441(19)	OW26-O16	2.64(4)
Zn1-O7	1.960(20)	Ca-OH17	2.448(18)		
<Zn-O>	1.927	Ca-O2	2.463(19)		
		Ca-OW23	2.480(19)		
Zn2-O16	1.898(19)	Ca-O3	2.543(17)		
Zn2-O9	1.912(20)	<Ca-O>	2.450		
Zn2-O4	1.932(17)				
Zn2-O7	1.965(18)				
<Zn-O>	1.927				

Table 6. Bond-valence analysis for falsterite (values are expressed in valence units*)

	Mg	Ca	Mn	Fe1	Fe2	Zn1	Zn2	P1	P2	P3	P4	H bonds	Σ
O1			0.42					1.34				+0.10	1.86
O2		0.26		0.43				1.29					1.98
O3		0.21			0.48			1.17					1.86
O4						0.50	0.54	1.08					2.12
O5		0.36							1.39				1.75
O6			0.22		0.45				1.27				1.94
O7						0.50	0.49		1.23				2.22
O8			0.26	0.51					1.06				1.83
O9							0.57			1.28		+0.21	2.06
O10										1.28		+0.20 +0.21 +0.08 +0.10	1.87
O11				0.38	0.36					1.25			1.99
O12	0.11					0.57				1.10			1.78
O13	0.09					0.63					1.41		2.13
O14											1.30	+0.23 +0.20 +0.18	1.91
O15				0.38	0.38						1.15		1.91
O16							0.59				1.05	+0.13 +0.10 +0.11	1.98
OH17		0.27		0.44	0.41							−0.14	0.98
OH18			0.32	0.39	0.43							−0.13	1.01
OW19			0.33									−0.23 −0.16 +0.17	0.11
OW20			0.25									−0.20 −0.17 +0.17	0.05
OW21		0.28										−0.20 −0.18 +0.14 +0.09	0.13
OW22		0.28										−0.10 −0.17 +0.17	0.18
OW23		0.25										−0.21 −0.17 +0.16	0.03
OW24	0.22 0.11											−0.21 −0.9	0.03
OW25	0.21											−0.08 −0.10	0.03
OW26	0.18											−0.10 −0.11	−0.03
Σ	0.92	1.91	1.80	2.53	2.51	2.20	2.19	4.88	4.95	4.91	4.91		

*Mg bond strengths correspond to half occupancy. Fe bond strengths are based on occupancy by ½ Fe^{2+} and ½ Fe^{3+}; Mg bond strengths are based on occupancy by 0.464 Mg^{2+} and 0.036 Zn^{2+}; Mg^{2+}–O, Ca^{2+}–O, Mn^{2+}–O, Fe^{2+}–O, Fe^{3+}–O, Zn^{2+}–O, and P^{5+}–O bond strengths from Brown and Altermatt (1985); hydrogen bond strengths based on O···O bond lengths are also from Brown and Altermatt (1985).

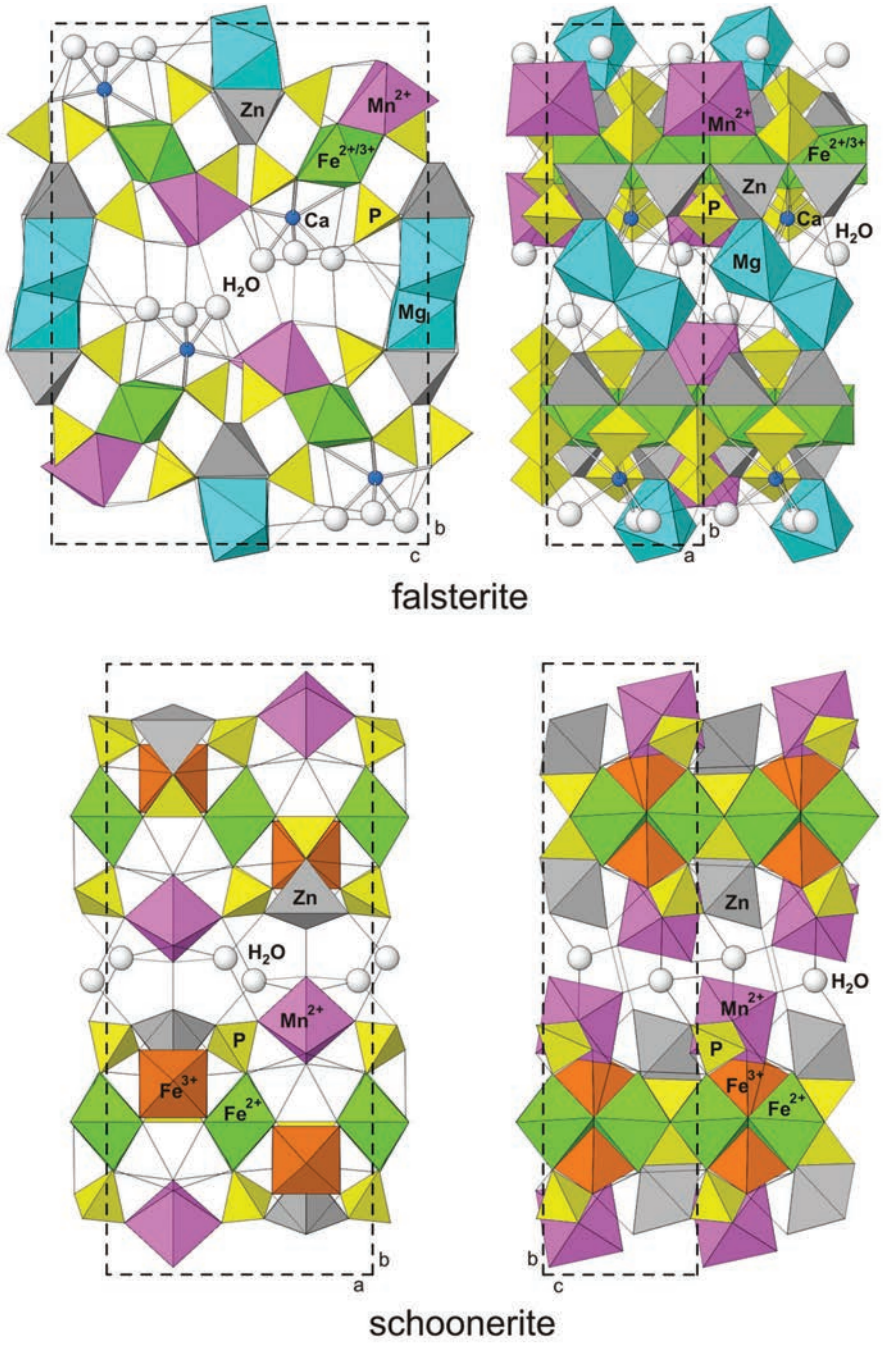

FIGURE 3. The crystal structures of falsterite and schoonerite. CaO_5 polyhedra are shown in ball-and-stick form. Hydrogen bonds are shown as thin black lines.

TABLE 7. Comparison of unit-cell parameters for falsterite, schoonerite, and jungite

	Falsterite	Schoonerite	Jungite
Ideal formula	$Ca_2MgMn^{2+}_2(Fe^{2+}_{0.5}Fe^{3+}_{0.5})_4Zn_4(PO_4)_8(OH)_4(H_2O)_{14}$	$Mn^{2+}Fe^{2+}_2Fe^{3+}Zn(PO_4)_3(OH)_2(H_2O)_7{\cdot}2H_2O$	$Ca_2Fe^{3+}_8Zn_4(PO_4)_9(OH)_9{\cdot}16H_2O$
Space group	$P2_1/c$	*Pmab*	*Pcmm*, $Pcm2_1$, or *Pc2m*
Unit-cell parameters			
a (Å)	6.3868(18)	11.119(4)	11.98(8)
b (Å)	21.260(7)	25.546(11)	20.37(10)
c (Å)	15.365(5)	6.437(3)	9.95(8)
β	90.564(6)°		

to the strong absorption typical of Fe^{2+}–Fe^{3+} charge transfer (cf. Mattson and Rossman 1987). By contrast, because Fe^{2+} and Fe^{3+} in the schoonerite structure are in separate sites that are linked across a single shared octahedral corner, Fe^{2+}–Fe^{3+} charge transfer does not occur and schoonerite exhibits an orange color and much less dramatic pleochroism. Furthermore, it is interesting from a paragenetic perspective that these two minerals occur in direct association at both falsterite localities.

Falsterite also bears some chemical similarity to jungite, $Ca_2Fe^{3+}_8Zn_4(PO_4)_9(OH)_9{\cdot}16H_2O$ (Moore and Ito 1980); however,

the structure of jungite is not known. The unit-cell parameters of falsterite, schoonerite, and jungite are compared in Table 7. The edge-sharing chains of FeO_6 octahedra in the structures of falsterite (along [100]) and schoonerite (along [001]) correspond to similar unit-cell parameters, 6.3868 and 6.437 Å, respectively, which equals twice the length of an octahedral edge. If the structure of jungite also contains such an edge-sharing chain, it may be along [100]. Note that half of the *a* unit-cell dimension in jungite, 5.99 Å, is significantly shorter than the aforementioned parameters in falsterite and schoonerite, but would be consistent with the Fe being all 3+ in jungite.

Acknowledgments

Associate editor Fernando Colombo, reviewer Frédéric Hatert, and an anonymous reviewer are thanked for their constructive comments on the manuscript. This study was funded by the John Jago Trelawney Endowment to the Mineral Sciences Department of the Natural History Museum of Los Angeles County.

References cited

Billings, M.P. (1956) The geology of New Hampshire. Part II. Bedrock geology. New Hampshire State Planning and Development Commission. 203.

Brown, I.D. and Altermatt, D. (1985) Bond-valence parameters from a systematic analysis of the inorganic crystal structure database. Acta Crystallographica, B41, 244–247.

Burla, M.C., Caliandro, R., Camalli, M., Carrozzini, B., Cascarano, G.L., De Caro, L., Giacovazzo, C., Polidori, G., and Spagna, R. (2005) SIR2004: an improved tool for crystal structure determination and refinement. Journal of Applied Crystallography, 38, 381–388.

Černý, P. and Ercit, T. (2005) The classification of granitic pegmatites revisited. Canadian Mineralogist, 43, 2005–2026.

Falster, A.U. (1981) Minerals of the Wausau Pluton. Mineralogical Record, 12, 93–97.

Falster, A.U., Simmons, W.B., and Webber, K.L. (1996) The Mineralogy and Geochemistry of the Animikie Red Ace Pegmatite, Florence County, Wisconsin. In S.G. Pandalai, Ed., Recent Research Developments in Mineralogy, p. 7–67. Research Signpost, Kerala, India.

Falster, A.U., Simmons, W.B., Webber, K.L., and Buchholz, T. (2000) Pegmatites and Pegmatite Minerals of the Wausau Complex, Marathon County, Wisconsin. Memorie della Società Italiana di Scienze Naturali e del Museo Civico di Storia Naturale di Milano, 30, 13–28.

Falster, A.U., Simmons, W.B., and Webber, K.L. (2001) Unorthodox compositional trends in columbite-group minerals from the Animikie Red Ace Pegmatite, Wisconsin, USA. Journal of the Czech Geological Society, 46, 69–79.

Falster, A.U., Buchholz, T.W., and Simmons, W.B. (2011) The Wausau Syenite Complex, Marathon Co., Wisconsin. Contributions to the 5th International Symposium on Granitic Pegmatites. Asociación Geológica Argentina, Serie D: Publicación Especial No. 14, 83–86.

Francis, C.A., Wise, M.A., Kampf, A.R., Brown, C.D., and Whitmore, R.W. (1993) Granitic pegmatites in New England. Fieldtrip Guidebook for the Northeastern U.S.: 1993 Boston GSA, vol, 1, E1–E24.

Frondel, C. (1941) Whitlockite: a new calcium phosphate, $Ca_3(PO_4)_2$. American Mineralogist, 26, 145–152.

——— (1949) Wolfeite, xanthoxenite and whitlockite from the Palermo mine, New Hampshire. American Mineralogist, 34, 692–705.

Frondel, C. and Ito, J. (1965) Composition of palermoite. American Mineralogist, 50, 777–779.

Kampf, A.R. (1977) Schoonerite: its atomic arrangement. American Mineralogist, 62, 250–255.

Lyons, J.B., Bothner, W.C., Moench, R.H., and Thompson, J.B. Jr. (1991) A new bedrock geologic map of New Hampshire. GSA Abstracts with Programs, 23, 60.

Mandarino, J.A. (1981) The Gladstone-Dale relationship: Part IV. The compatibility concept and its application. Canadian Mineralogist, 19, 441–450.

Martin, R.F. and Falster, A.U. (1986) Proterozoic Sanidine and Microcline in Pegmatite, Wausau Complex, Wisconsin. Canadian Mineralogist, 24, 709–716.

Mattson, S.M. and Rossman, G.R. (1987) Identifying characteristics of charge transfer transitions in minerals. Physics and Chemistry of Minerals, 14, 94–99.

McManus, C.E., McMillan, N.J., Harmon, R.S., Whitmore, R.W., De Lucia, F.C. Jr., and Miziolek, A.W. (2008) Use of laser induced breakdown spectroscopy in the determination of gem provenance: beryls. Applied Optics, 47, G72–G79.

Moore, P.B. and Ito, J. (1980) Jungit und Matulait: zwei neue taflige Phosphat-Mineralien. Aufschluss, 31, 55–61.

Moore, P.B. and Kampf, A.R. (1977) Schoonerite, a new zinc-manganese-iron phosphate mineral. American Mineralogist, 62, 246–249.

Moore, P.B., Lund, D.H., and Keester, K.L. (1973) Bjarebyite, (Ba,Sr)$(Mn,Fe,Mg)_2Al_2(OH)_3(PO_4)_3$, a new species. Mineralogical Record, 4, 282–285.

Moore, P.B., Kampf, A.R., and Irving, A.J. (1974) Whitmoreite, $Fe^{2+}Fe^{3+}(OH)_2(H_2O)_4(PO_4)_2$, a new species: Its description and atomic arrangement. American Mineralogist, 59, 900–905.

Moore, P.B., Irving, A.J., and Kampf, A.R. (1975) Foggite, $CaAl(OH)_2(H_2O)[PO_4]$; goedkenite, $(Sr,Ca)_2Al(OH)[PO_4]_2$; and samuelsonite, $(CaBa)Fe^{2+}Mn^{2+}Ca_8Al_2(OH)_2[PO_4]_{10}$: Three new species from the Palermo No. 1 pegmatite, North Groton, New Hampshire. American Mineralogist, 60, 957–964.

Nizamoff, J.W., Whitmore, R.W., Falster, A.U., and Simmons, W.B. (2007) Parascholzite, keckite, gormanite and other previously unreported secondary species and new data on kulanite and phosphophyllite from the Palermo no. 1 mine, North Groton, New Hampshire. Rocks and Minerals, 82, 145.

Segeler, C.G., Ulrich, W., Kampf, A.R., and Whitmore, R.W. (1981) Phosphate minerals of the Palermo No. 1 pegmatite. Rocks and Minerals, 56, 197–214.

Sheldrick, G.M. (2008) SHELXL97—Program for the refinement of crystal structures. University of Göttigen, Germany.

Strunz, H., Forster, A., and Tennyson, C. (1975) Die Pegmatite der nördlichen Oberpfalz. Aufschluss, 26, 117–189.

Thompson, W.B., Bearss, G.T., Falster, A.U., Simmons, W.B., and Nizamoff, J.W. (2000) The Estes Quarry, Cumberland County, Maine. Rocks and Minerals, 75, 408–418.

Whitmore, R.W. and Lawrence, R.C. Jr. (2004) The Pegmatite Mines Known as Palermo. Friends of Palermo Mines, North Groton, New Hampshire, 219 p.

Manuscript received September 20, 2011
Manuscript accepted December 31, 2011
Manuscript handled by Fernando Colombo